Polarized Optical Absorption and Emission of Pt(II) Complexes: Single Crystal $[Pt(o\text{-}phen)(en)]Cl_2 \cdot 2\,H_2O$

R. Schwarz and G. Gliemann

Institut für Physikalische und Theoretische Chemie, Universität Regensburg, Universitätsstr. 31, Regensburg, FRG

Z. Naturforsch. **44 a**, 99–105 (1989); received November 23, 1988

The influence of temperature ($1.9 \leqq T \leqq 295$ K) on the polarized optical absorption and emission spectra of single crystal $[Pt(o\text{-}phen)(en)]Cl_2 \cdot 2\,H_2O$ is reported. Analysis of the spectra shows that the emission at low temperatures originates from the states of three types of traps located energetically by $\Delta\bar{\nu} \lesssim 5\ cm^{-1}$, 43 cm^{-1}, and 194 cm^{-1}, respectively, below the triplet exciton band.

Introduction

Numerous articles on the photophysics and photochemistry of solutions of transition metal complexes with polypyridine ligands such as 1,10-phenanthroline (o-phen) and 2,2′-bipyridine (bipy) have been published in the last two decades [1–12]. Depending on the central ion and/or the heterocycle, the energetically lowest excited electronic states of these systems were assigned to metal-centered (LF) states, ligand-centered (LC) states, or metal-to-ligand charge-transfer (MLCT) states [1–8]. Sometimes even a substitution at the heterocycle [8–10] or a variation of the solvens changes the type of the lowest excited states [11, 12].

Recently we reported on the optical properties of single crystal $[Pt(CN)_2L]$, with L = o-phen or bipy [13, 14]. In both systems the spectral position, the intensity, and the lifetime of the emission depend on the temperature and on the strength of an applied magnetic field. From this behavior the type of low-energy optical transitions and the energy order as well as the symmetry of the emitting states could be deduced. The resulting energy level diagrams are very similar to the one that has been developed for single crystals of tetracyanoplatinate(II) complexes (TCP), which exhibit quasi-one-dimensional structures [15–18]. Typical features of the TCP energy level diagram are due to a strong intercomplex coupling in the solid state. In the case of $[Pt(CN)_2L]$ such a coupling is also effective, causing a change of the lowest excited states from the LC type (glass) to the MLCT type (single crystal), which leads to an increase of spin-orbit coupling. Several of the magnetic field and temperature effects mentioned above can be explained by this increase.

Unlike TCP and $[Pt(CN)_2L]$, the compound $[Pt(o\text{-}phen)(en)]Cl_2 \cdot 2\,H_2O$ forms single crystals with a relatively large separation between neighboring complex units, indicating a weak intercomplex coupling. The purpose of this paper is to describe the temperature dependence of the solid-state absorption and luminescence of $[Pt(o\text{-}phen)(en)]Cl_2 \cdot 2\,H_2O$ and, furthermore, the behavior of the luminescence under applied magnetic fields. To rationalize the experimental results, a model of the electronic structure of the solid will be established and compared with the energy level diagram of single crystals TCP and $[Pt(CN)_2L]$.

Experimental

Single crystals of $[Pt(o\text{-}phen)(en)]Cl_2 \cdot 2\,H_2O$ were synthesized by a procedure described in [19, 20]. The yellow crystals are needle shaped with the crystallographic *a* axis parallel to the needle axis.

The apparatus for the polarized absorption spectroscopy, the polarized emission spectroscopy, and the lifetime measurements have been described in [15] and [21]. The crystal luminescence was excited by the 364 nm line of an argon-ion laser.

Reprint requests to Prof. Dr. G. Gliemann, Institut für Physikalische und Theoretische Chemie, Universität Regensburg, Universitätsstraße 31, D-8400 Regensburg.

0932-0784 / 89 / 0200-0099 $ 01.30/0. – Please order a reprint rather than making your own copy.

Dieses Werk wurde im Jahr 2013 vom Verlag Zeitschrift für Naturforschung in Zusammenarbeit mit der Max-Planck-Gesellschaft zur Förderung der Wissenschaften e.V. digitalisiert und unter folgender Lizenz veröffentlicht: Creative Commons Namensnennung-Keine Bearbeitung 3.0 Deutschland Lizenz.

This work has been digitalized and published in 2013 by Verlag Zeitschrift für Naturforschung in cooperation with the Max Planck Society for the Advancement of Science under a Creative Commons Attribution-NoDerivs 3.0 Germany License.

Zum 01.01.2015 ist eine Anpassung der Lizenzbedingungen (Entfall der Creative Commons Lizenzbedingung „Keine Bearbeitung") beabsichtigt, um eine Nachnutzung auch im Rahmen zukünftiger wissenschaftlicher Nutzungsformen zu ermöglichen.

On 01.01.2015 it is planned to change the License Conditions (the removal of the Creative Commons License condition "no derivative works"). This is to allow reuse in the area of future scientific usage.

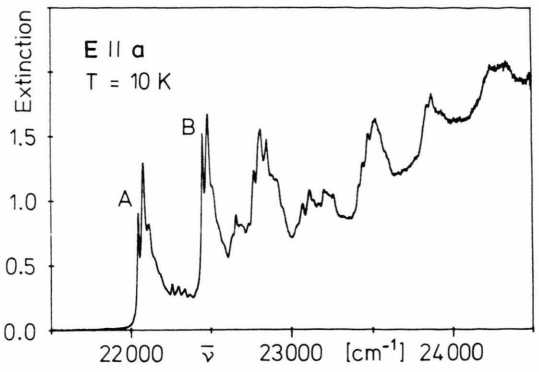

Fig. 1. $E \parallel a$ polarized absorption spectrum of single crystal $[Pt(o\text{-phen})(en)]Cl_2 \cdot 2\,H_2O$ at $T = 10$ K. Thickness of the crystal: 30 μm.

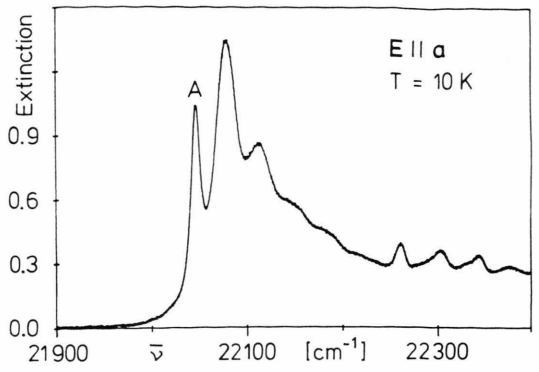

Fig. 2. Expanded low-energy section of the $E \parallel a$ polarized absorption spectrum of single crystal $[Pt(o\text{-phen})(en)]Cl_2 \cdot 2\,H_2O$ at $T = 10$ K. Thickness of the crystal: 30 μm.

Results

Fig. 1 shows the low-temperature, $E \parallel a$-polarized absorption spectrum of single crystal $[Pt(o\text{-phen})(en)]Cl_2 \cdot 2\,H_2O$. E is the electric field vector of the light, a denotes the direction of the crystallographic a axis. The spectrum is composed of a sequence of band groups which display a distinct fine structure. As an example, Fig. 2 represents the band group of lowest energy in an expanded scale. The absorption line A has its maximum at about $\bar{\nu} = 22\,065$ cm^{-1} and a half-width of $\Delta\bar{\nu} \sim 30$ cm^{-1}. Assuming that the molar concentration of $[Pt(o\text{-phen})(en)]Cl_2 \cdot 2\,H_2O$ in the crystal is in the same order as that of $[PtCl_2(bipy)]$ ($c = 6.2$ mol · l^{-1}, [22]), the extinction coefficient of this line can be estimated as $\varepsilon \sim 60$ l · mol^{-1} · cm^{-1}. A characteristic feature of this low-energy band group is its structure formed by equidistant bands. These bands have half-widths of ~ 60 cm^{-1} and their maxima are separated by $\Delta\bar{\nu} = 32$ cm^{-1}. In contrast to the $E \parallel a$ absorption, the $E \perp a$ polarized absorption spectrum exhibits no comparable structure and has a distinctly lower extinction.

The polarized emission spectra at $T = 1.9$ K are shown in Figure 3. Both spectra have a very similar shape, however the $E \parallel a$ emission is by a factor of ~ 5 more intense than the $E \perp a$ emission. The spectra are composed of non-equidistant band groups which exhibit marked fine structure. In order to demonstrate structural details and the spectral position of the fine structure lines, the upper part of Fig. 4 shows an expanded plot of the high-energy flank of the $E \parallel a$ emission at $T = 1.9$ K. Within the limits of experimental error, the emission line labeled by 1 coincides energetically with line A at the low-energy flank of the $E \parallel a$ absorption spectrum, cf. Figure 2. At the red side of peak 1, two further lines shifted by $\Delta\bar{\nu} = 43$ cm^{-1} and $\Delta\bar{\nu} = 194$ cm^{-1}, respectively, are resolved. Corresponding triplets of peaks can be identified also at the spectral positions 2–6. In Table 1 the energies of the

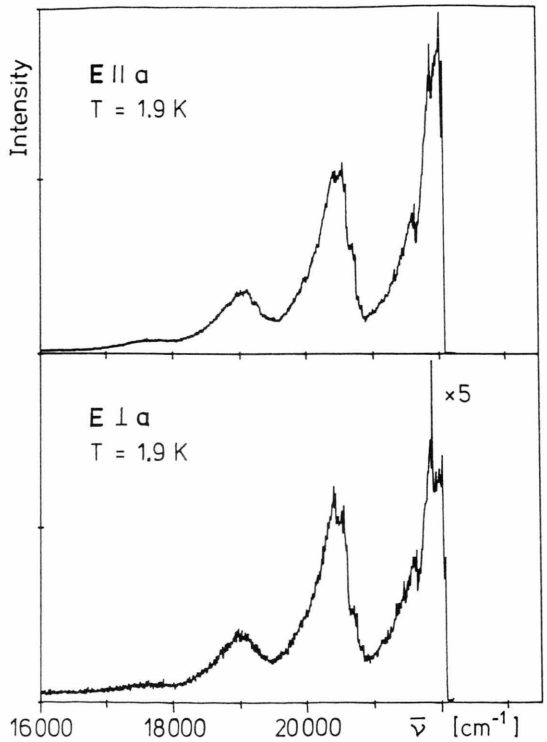

Fig. 3. Polarized emission spectra of single crystal $[Pt(o\text{-phen})(en)]Cl_2 \cdot 2\,H_2O$ at $T = 1.9$ K. $\lambda_{exc} = 364$ nm.

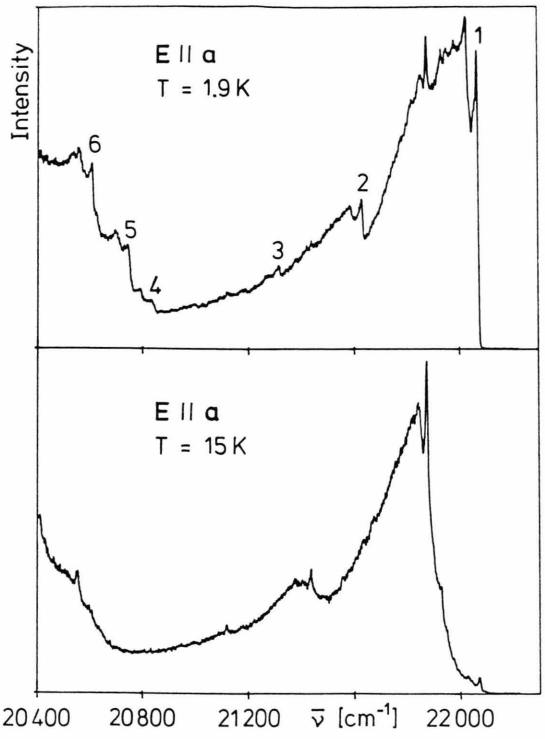

Fig. 4. Expanded high-energy section of the $\boldsymbol{E} \parallel \boldsymbol{a}$ polarized emission spectrum of single crystal [Pt(o-phen)(en)]$Cl_2 \cdot 2\,H_2O$ at $T = 1.9$ K and 15 K. $\lambda_{exc} = 364$ nm.

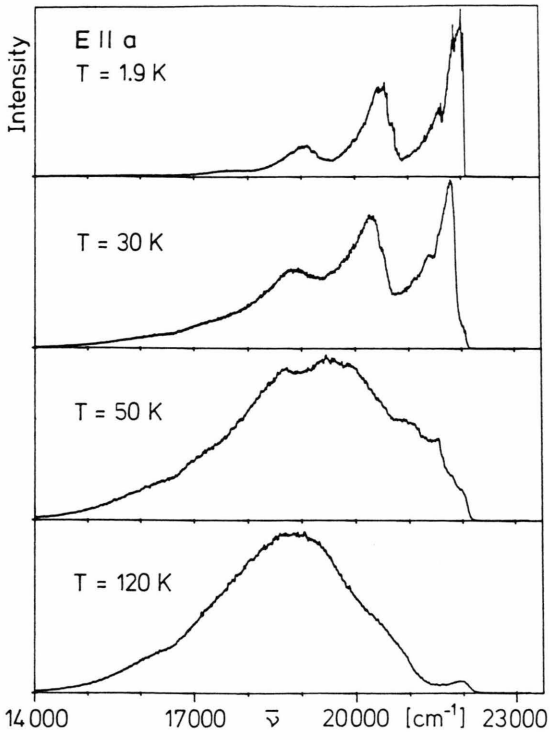

Fig. 5. $\boldsymbol{E} \parallel \boldsymbol{a}$ polarized emission spectra of single crystal [Pt(o-phen)(en)]$Cl_2 \cdot 2\,H_2O$ at $T = 1.9$ K, 30 K, 50 K, and 120 K. Intensities in arbitrary units. $\lambda_{exc} = 364$ nm.

Table 1. Energy $\bar{\nu}$ and energy separation $\Delta\bar{\nu}$ (relative to peak 1) of the fine structure peaks labeled in Figure 4. $\bar{\nu}_a$ and $\bar{\nu}_b$ are vibrational energies [23] of $[Rh(o\text{-phen})_3]^{3+}$ and o-phen, respectively.

Peak	$\bar{\nu}$ [cm^{-1}]	$\Delta\bar{\nu}$ [cm^{-1}]	$\bar{\nu}_a$ [cm^{-1}]	$\bar{\nu}_b$ [cm^{-1}]
1	22 065			
2	21 624	441	436	414
3	21 313	752	739	
4	20 830	1235	1210	1299
5	20 739	1326	1308	1407
6	20 604	1461	1455	

labeled fine structure lines and their energy separations are listed. The last two columns of Table 1 contain values of vibrational energies [23] of $[Rh(o\text{-phen})_3]^{3+}$ and o-phen, respectively.

The influence of temperature on the luminescence of single crystal [Pt(o-phen)(en)]$Cl_2 \cdot 2\,H_2O$ is summarized in Figs. 4–6. Temperature increase yields the following effects. Between $T = 1.9$ K and 30 K the coarse structure due to the band groups is preserved but the fine structure within the groups vanishes, cf. Figure 5. When the temperature is raised to $T = 50$ K a broad phosphorescence band appears. At $T = 120$ K the luminescence consists of two distinctly separated bands, a broad intense one with maximum at $\bar{\nu} \approx 19\,000$ cm^{-1} and a weaker band at $\bar{\nu} = 21\,946$ cm^{-1}. Further increase of temperature to room temperature induces a red-shift of the broad emission band.

The behavior of the fine structure between $T = 1.9$ K and 15 K is demonstrated in Figure 4. The intensity scales of both spectra are comparable. A comparison of the line patterns shows that with increasing temperature the two peaks at the high-energy edge of the spectrum lose intensity, successively one by one, beginning with the line of highest energy (label 1). Simultaneously with these two peaks, the corresponding lines at the positions 2 to 6 disappear. The respective red components of the above mentioned triplets of peaks, however, preserve their intensity during this temperature variation. As to its shape, the $T = 15$ K spectrum resembles closely to the $T = 1.6$ K phosphorescence spectra of the complex $[Rh(o\text{-phen})_3]^{3+}$ and the free ligand o-phen [23].

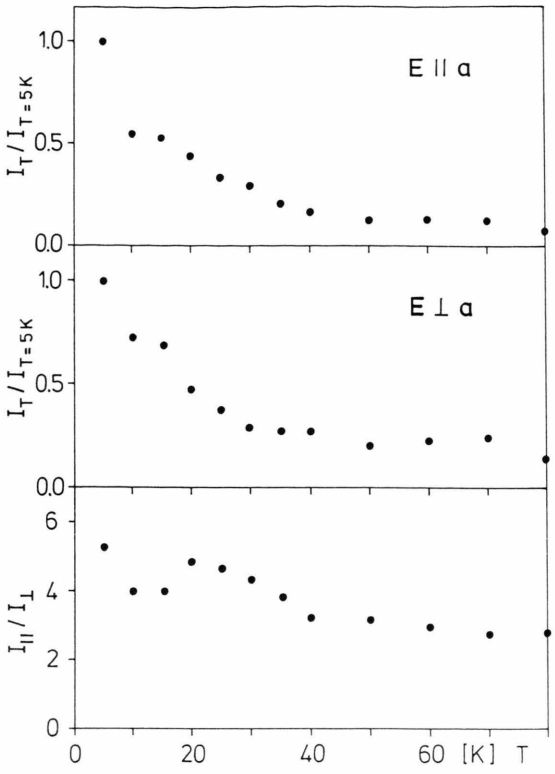

Fig. 6. Relative intensities $I_T/I_{T=5\,K}$ and intensity ratio $I_{\parallel}/I_{\perp}$ of the polarized emission of single crystal $[Pt(o\text{-}phen)(en)]Cl_2 \cdot 2\,H_2O$ as functions of temperature. $\lambda_{exc} = 364$ nm.

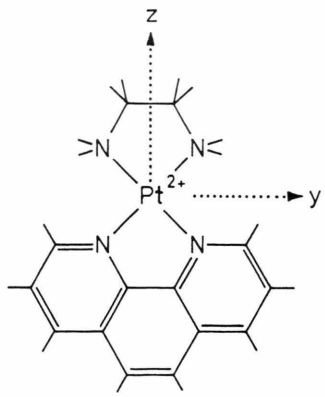

Fig. 7. Proposed structure of $[Pt(o\text{-}phen)(en)]^{2+}$. The axes x and a are perpendicular to the plane of the complex.

Raising the temperature from $T = 5$ K to 40 K lowers the integral intensity by a factor of ~ 5, whereas the ratio of the intensities $I_{\parallel}$ and $I_{\perp}$, belonging to the polarizations $\boldsymbol{E} \parallel \boldsymbol{a}$ and $\boldsymbol{E} \perp \boldsymbol{a}$, respectively, is reduced from ~ 5 to ~ 3, cf. Figure 6. By further increase of temperature the integral quantum yields are not affected appreciably.

The decay curves of the polarized emission determined at $T = 1.9$ K are mono-exponential and yield a lifetime of $\tau = 95$ μs. This value is independent of the direction of polarization and has been found at every emission wavelength. On raising the temperature the emission displays a non-mono-exponential and faster decay.

The emission of single crystal $[Pt(o\text{-}phen)(en)]Cl_2 \cdot 2\,H_2O$ cannot be influenced by homogeneous magnetic fields with field strengths $H \leqq 6$ T.

Discussion

Reports on the crystal structure of $[Pt(o\text{-}phen)(en)]Cl_2 \cdot 2\,H_2O$ are not available but the crystallographic data of similar compounds with polypyridine ligands, e.g. $[PtCl_2(bipy)]$, are known [22]. Accordingly the following features of the structure of single crystal $[Pt(o\text{-}phen)(en)]Cl_2 \cdot 2\,H_2O$ will be assumed. The complex cations $[Pt(o\text{-}phen)(en)]^{2+}$ have the symmetry C_{2v}, cf. Figure 7. In the crystal the planes of the cations are arranged parallel. The molecular axis x, the needle axis of the crystal and crystallographic a axis are parallel. The intercomplex coupling is weak.

By the ligand field of symmetry C_{2v} the degeneracy of the five metal d-states is partly removed. The resulting states have the following energetic order [13, 14, 22]:

$$1a_1(x^2) < 1b_1(xz),\ 1a_2(xy) < < 2a_1(x^2 - z^2) \ll 1b_2(yz).$$

The HOMO and LUMO of the heterocycle o-phen are due to pairs of nearly degenerate orbitals $a_2(\pi)$, $b_1(\pi)$ and $b_1(\pi^*)$, $a_2(\pi^*)$, respectively [23, 24].

As shown in the previous section and as will be confirmed in the following discussion the luminescence of $[Pt(o\text{-}phen)(en)]Cl_2 \cdot 2\,H_2O$ at $T = 15$ K is comparable to the 1.6 K-phosphorescence of complex $[Rh(o\text{-}phen)_3]^{3+}$ as well as of the free ligand o-phen. With respect to this similarity the HOMO and LUMO of the heterocycle o-phen is expected to constitute the HOMO and LUMO of the total complex $[Pt(o\text{-}phen)(en)]Cl_2$, respectively. For symmetry reasons an admixture of the metal-d-states $1b_1(xz)$ and $1a_2(xy)$ to the HOMO and to the LUMO is possible, yielding a partial metal character of these states.

Taking electron interaction into account, the electron ground state configuration of a single complex forms the term $^1A_1$. The lowest excited terms $^3B_2$ and $^1B_2$ result from a mixed configuration of the type [23]

$$\alpha[b_1(\pi)\, a_2(\pi^*)] + \beta[a_2(\pi)\, b_1(\pi^*)].$$

By weak intercomplex coupling in the solid state the electronic terms $^1B_2$ and $^3B_2$ form small exciton bands. In order to rationalize the observed optical properties of single crystal [Pt(o-phen)(en)]$Cl_2 \cdot 2H_2O$ the existence of three distinct types of X-traps, T_1, T_2, and T_3, is postulated. The X-traps can be assigned to [Pt(o-phen)(en)]Cl_2 complexes which are disturbed directly or indirectly (second coordination sphere) by impurities and lattice defects, respectively. Traps of different types have different energy levels, located below the respective exciton band. Figure 8 illustrates schematically the resulting energy level diagram for the triplet states. Corresponding models for single crystals have been established to describe the optical properties of purely organic compounds [25–27] as well as of transition metal chelate complexes with aromatic ligands [28–30].

The polarized absorption band A, cf. Fig. 2, is assigned to the ligand-centered 0–0-transition from the electronic ground state $^1A_1$ to the $^3B_2$ exciton band. The partial metal character of the HOMO and LUMO weakens the spin selection rule via spin-orbit coupling thus yielding the oscillator strength of the absorption band ($\varepsilon \sim 60\, l \cdot mol^{-1} \cdot cm^{-1}$). In the low-energy part of the absorption spectrum, cf. Fig. 2, a phonon progression of energy $\Delta\bar{\nu} = 32\ cm^{-1}$ coupled to the 0–0-transition (band A) is observed. As shown in Fig. 1, the band groups of higher energy have a similar shape as the low-energy band group. They result from the latter by the addition of intracomplex vibration quanta, e.g. $\bar{\nu}_{vib} \sim 415\ cm^{-1}$ (band B) and $\bar{\nu}_{vib} \sim 735\ cm^{-1}$ (band C), which can be assigned to vibrations of the electronic excited ligand o-phen, cf. Table 1.

The emission properties at low temperatures ($T < 30$ K) can be traced back to the radiative deactivation of three different types of X-traps, T_1, T_2 and T_3. After the excitation of the crystal and subsequent non-radiative deactivation into the $^3B_2$ exciton band, the energy is transferred rapidly within this band and may be trapped with a rate constant $k_{ni} \gg k_E$ at one of the defect states, cf. Figure 8. Because of the low concentration of the traps, a direct energy transfer between the distinct traps via the Förster-Dexter mechanism is

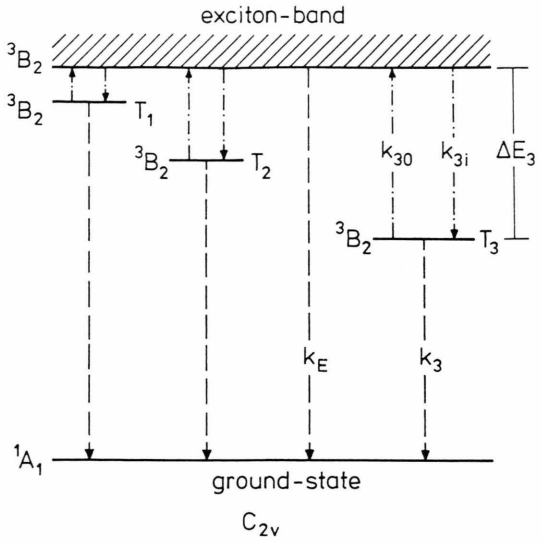

Fig. 8. Energy level diagram of the lowest electronic states of single crystal [Pt(o-phen)(en)]$Cl_2 \cdot 2H_2O$ (schematic). T_1: trap type 1; stabilization energy $\Delta E_1 \leqq 5\ cm^{-1}$. T_2: trap type 2; stabilization energy $\Delta E_2 = 43\ cm^{-1}$. T_3: trap type 3; stabilization energy $\Delta E_3 = 194\ cm^{-1}$. The corresponding rate constants for emission (k_n), trapping (k_{ni}) and detrapping (k_{n0}) are indicated.

not probable. Thus, energy transfer between the traps is expected to proceed indirectly via the exciton band. At $T = 1.9$ K such a thermally activated energy transfer will be ineffective, and the emission is the superposition of the luminescence of all three types of traps. The three sharp lines highest in energy, cf. Fig. 4, represent the corresponding zero-phonon transitions of the different traps. From the spectral positions of these 0–0-transitions the depths of the traps T_2 and T_3 relative to the T_1-level follow as $\Delta\bar{\nu} = 43\ cm^{-1}$ and $194\ cm^{-1}$, respectively. With regard to the limits of experimental error the depth of the T_1 traps is expected to be smaller than $5\ cm^{-1}$. The observed vibrational frequencies, labeled by 2–6 in Fig. 4, are comparable to those reported for single crystal $[Rh(o\text{-phen})_3]^{3+}$ and are different from those of the free heterocycle o-phen, as shown in Table 1 [23]. Combined effects of the changes in force constants and effective masses due to complex formation presumably produce these shifts. Following [23], the $441\ cm^{-1}$ frequency is assigned to a ring-bending mode, while the frequencies $1235\ cm^{-1}$ and $1461\ cm^{-1}$ belong to C=C(N) stretching vibrations.

In accordance with the model whereupon the X-traps are weakly disturbed $[Pt(o\text{-phen})(en)]^{2+}$ complex units, the emission lifetime τ is independent of the

detection wavelength. The value $\tau = 95\ \mu s$ is much lower than that of the complex $[Rh(o\text{-phen})_3]^{3+}$ ($\tau = 30.6$ ms) and that of the free ligand o-phen ($\tau = 1.4$ s) [23]. The increase of the corresponding decay rate of the Pt-complex is an effect of the external spin-orbit-coupling due to the heavy metal Pt.

On raising the temperature, the traps will be depopulated by thermal activation into the exciton band and the energy transfer mentioned above becomes probable. According to the strong temperature dependence of the detrapping rate constants k_{n0} and the different stabilization energies ΔE_n, the detrapping of the defect states T_1, T_2, T_3 is effective at different temperatures. With increase of temperature to $T = 15$ K, depopulation via the pathway of thermal activation becomes dominant successively for the traps T_1 and T_2, and the corresponding zero-phonon transitions with their vibronic satellites disappear in the emission spectra, cf. Figure 4. Thus, at $T = 15$ K only the deepest traps T_3, stabilized by $\Delta\bar{\nu} = 194\ cm^{-1}$, are occupied and determine the luminescence. This situation is equivalent to a crystal containing only one emitting species. That explains that the phosphorescence spectra of single crystal $[Pt(o\text{-phen})(en)]Cl_2 \cdot 2\ H_2O$ at $T = 15$ K resemble the emission spectra of crystals $[Rh(o\text{-phen})_3]^{3+}$ and o-phen at $T = 1.6$ K [23], which indicate no defect state properties. Further increase of temperature to $T = 50$ K establishes thermal equilibrium between all the X-traps (T_1, T_2, T_3) and the exciton band. The unstructured emission spectra at $T = 50$ K, cf. Fig. 5, are superpositions of the luminescence of all types of traps and of the radiative deactivation of the $^3B_2$ exciton band. At $T > 50$ K the phosphorescence of the exciton band dominates the emission spectra, as shown in Figure 5.

The reduction of the integral quantum yield between $T = 1.9$ K and 40 K is assigned to the inefficiency of the system to transfer the energy via the exciton band from the shallow traps T_1 and T_2 to the deep traps T_3, cf. Figure 6. Quantitative calculations concerning the population-depopulation kinetics of the traps and the excition band confirm the temperature dependence of the emission lifetime and of the intensities of the zero-phonon lines [25, 31–33]. In the underlying model it is assumed that shallow traps S and deep traps D are coupled via the exciton band and that the detrapping rate constants k_{n0} vary with temperature as $k_{n0} = k_{n0}^0 \cdot \exp(-\Delta E_n/kT)$ with ΔE_n the trap depth. The calculations yield the following results. At temperatures too low to depopulate the deep traps and the shallow traps ($k_{d0} = k_{s0} = 0$), the intensity ratio of the corresponding zero-phonon lines reflects the ratio of the numbers of both traps, and the emission lifetimes at the zero-phonon lines are equal. In the range of temperature which enables the depopulation of the shallow traps but not of the deep traps ($k_{s0} \gg 0$, $k_{d0} = 0$) the logarithmic plot of the intensity ratio I_d/I_s varies as $-\Delta E_s/kT$ with $I_d = \text{const}$. Furthermore, the decay rates of the shallow traps are dominated by the rates of the competing mechanism of trapping and detrapping. Experiments that support these predictions are reported for crystalline organic compounds [25–27] and for transition metal complexes [28–30].

Our experimental results for $1.9\ K \leqq T \lesssim 15\ K$ described in the previous section harmonize with the theory too. At $T = 1.9$ K the decay curves are mono-exponential and independent of the emission wavelength, whereas at higher temperatures the emission displays a faster non-mono-exponential dacay. At $T \gtrsim 15$ K, the intensity of the zero-phonon line, which belongs to the deep traps T_3, remains constant and the transitions due to the shallow traps T_1 and T_2 vanish completely.

The polarization properties of the emission and the independence of the emission on external magnetic fields can be understood if the spin-orbit coupling is taken into account. It removes the triplet degeneracy of the lowest excited states of the traps T_1, T_2, and T_3, as $^3B_2 \rightarrow A_1' + A_2' + B_1'$. The experimental data are compatible with this result if the spin-orbit components have the energy order $E(A_2') > E(A_1') \approx E(B_1')$ with a splitting $A_1' - B_1'$ smaller than $1\ cm^{-1}$ (limit of resolution). Then, the electric dipole transitions between the ground state $A_1'(^1A_1)$ and the excited states $A_1'(^3B_2)$ and $B_1'(^3B_2)$ are allowed with polarizations $\boldsymbol{E} \perp \boldsymbol{a}$ and $\boldsymbol{E} \parallel \boldsymbol{a}$, respectively. This explains that both polarizations are observed in the emission spectrum. Moreover, since the radiative transitions between the lowest spin-orbit components of the triplets $^3B_2$ and the ground state are allowed already at zero field, an external magnetic field will not change the emission properties perceptibly, neither at $\boldsymbol{H} \parallel \boldsymbol{a}$ (symmetry C_s) nor at $\boldsymbol{H} \perp \boldsymbol{a}$ (symmetry C_2), as can be shown straightforwardly by symmetry analysis.

Acknowledgements

This research has been supported by the Deutsche Forschungsgemeinschaft and the Fonds der Chemischen Industrie.

[1] J. N. Demas, J. Chem. Educ. **60,** 803 (1983).
[2] M. K. De Armond, Coord. Chem. Rev. **36,** 325 (1981).
[3] K. Kalyanasundaram, Coord. Chem. Rev. **46,** 159 (1982).
[4] R. J. Watts, J. Chem. Educ. **60,** 834 (1983).
[5] M. A. Jamieson, N. Serpone, and M. Z. Hoffman, Coord. Chem. Rev. **39,** 121 (1981).
[6] N. Serpone and M. Z. Hoffman, J. Chem. Educ. **60**, 853 (1983).
[7] A. Juris, F. Barigelletti, V. Balzani, and A. v. Zelewsky, Inorg. Chem. **24,** 202 (1985).
[8] V. Balzani, F. Bolletta, M. T. Gandolfi, and M. Maestri, Top. Curr. Chem. **75,** 1 (1978).
[9] G. A. Crosby, Acc. Chem. Res. **8,** 231 (1975).
[10] G. A. Crosby, J. Chem. Educ. **60,** 791 (1983).
[11] R. J. Watts, G. A. Crosby, and J. L. Sansegret, Inorg. Chem. **11,** 1474 (1972).
[12] R. J. Watts and G. A. Crosby, Chem. Phys. Lett. **13,** 619 (1972).
[13] R. Schwarz, M. Lindner, and G. Gliemann, Ber. Bunsenges. Phys. Chem. **91,** 1233 (1987).
[14] J. Biedermann, M., Wallfahrer, and G. Gliemann, J. Luminescence **37,** 323 (1987).
[15] J. Hidvegi, W. v. Ammon, and G. Gliemann, J. Chem. Phys. **76,** 4361 (1982).
[16] W. v. Ammon, I. Hidvegi, and G. Gliemann, J. Chem. Phys. **80,** 2837 (1984).
[17] W. v. Ammon and G. Gliemann, J. Chem. Phys. **77,** 2266 (1982).
[18] G. Gliemann and H. Yersin, Struct. Bonding, Berlin **62,** 87 (1985).
[19] K. D. Hodges and J. V. Rund, Inorg. Chem. **14,** 525 (1975).
[20] J. R. Hall and R. A. Plowman, Aust. J. Chem. **9,** 143 (1956).
[21] W. Tuszynski and G. Gliemann, Ber. Bunsenges. Phys. Chem. **89,** 940 (1985).
[22] M. Textor and H. R. Oswald, Z. anorg. allg. Chem. **407,** 244 (1974).
[23] Y. Komada, S. Yamauchi, and N. Hirota, J. Phys. Chem. **90,** 6425 (1986).
[24] C. C. Phifer and D. R. McMillin, Inorg. Chem. **25,** 1329 (1986).
[25] M. Vala, J. Baiardo, A. Wierzbicki, and J. Trajberg, Chem. Phys. **116,** 221 (1987).
[26] G.Weinzierl and J. Friedrich, Chem. Phys. Lett. **83,** 204 (1981).
[27] Y. Komada, S. Yamauchi, and N. Hirota, J. Chem. Phys. **82,** 1651 (1985).
[28] R. Schwarz, G. Gliemann, L. Chassot, and A. v. Zelewsky, Inorg. Chem., in press.
[29] R. Schwarz, G. Gliemann, Ph. Jolliet, and A. v. Zelewsky, Inorg. Chem., in press.
[30] R. Schwarz, G. Gliemann, L. Chassot, Ph. Jolliet, and A. v. Zelewsky, Helvet. Chim. Acta, in press.
[31] M. D. Fayer and C. B. Harris, Phys. Rev. **B 9,** 748 (1974).
[32] R. M. Shelby, A. H. Zewail, and C. B. Harris, J. Chem. Phys. **64,** 3192 (1976).
[33] W. Güttler, J. U. v. Schütz, and H. C. Wolf, Chem. Phys. **24,** 159 (1977).